Rare Met. (2022) 41(6):2084–2093
https://doi.org/10.1007/s12598-021-01935-6

RARE METALS

ORIGINAL ARTICLE

Engineering of electrolyte ion channels in MXene/holey graphene electrodes for superior supercapacitive performances

Zhuo Cai, Yi-Fei Ma*, Mei Wang*, A.-Niu Qian, Zhao-Min Tong, Lian-Tuan Xiao, Suo-Tang Jia, Xu-Yuan Chen

Received: 9 October 2021 / Revised: 5 November 2021 / Accepted: 11 November 2021 / Published online: 28 February 2022

Abstract MXene has given great promises to supercapacitor electrode material due to its high conductivity and redox properties. However, the self-agglomeration of the MXene lamella will reduce its contact area with the electrolyte and generate a tortuous transportation pathway of the electrolyte ions, thereby reducing its capacitive performance and rate capability. In this work, we engineered the electrolyte ion channels by adjusting the MXene lamella size and inserting holey graphene (HG) nanosheets into the interlayer of the MXene flakes. The developed MXene/HG electrode can not only avoid the self-restacking of MXene but also provide unimpeded ion transport channels. As a result, the supercapacitive and rate performances of the small MXene lamella-based MXene/HG (S-MXene/HG) supercapacitor are prominently ameliorated. By adjusting the content of HG, the S-MXene/$HG_{0.05}$ electrode exhibits excellent gravimetric capacitance of 446 $F{\cdot}g^{-1}$ and a rate capability of 77.5%. The S-MXene/$HG_{0.05}$-based symmetric supercapacitor provides an impressive energy density of 14.84 $Wh{\cdot}kg^{-1}$ with excellent cyclic stability of 96% capacitance retention after 10,000 cycles. This demonstration of the engineering of the ion channels shows great potential in two-dimensional material-based supercapacitor electrodes.

Keywords MXene; Holey graphene; Supercapacitor; Ion channel

1 Introduction

Among the supercapacitor electrode materials, $Ti_3C_2T_x$ MXene nanosheets have a series of advantages including high flexibility, easy dispersion in water, high pseudo-capacitance activity originated from the fast surface redox reactions capacitance, leading to their huge potentials in energy storage devices [1–4]. So far, MXene-based electrodes have been fabricated via various methods including vacuum filtration [5], spray coating [6], electrophoretic deposition (EPD) [7], spin coating [8], etc. Among these preparation methods, the vacuum filtration method is simpler and easier to obtain flexible MXene membranes. However, it still remains challenging that the MXene flakes are easy to self-agglomerate during the manufacturing process, which causes the sluggish ion diffusion and poor rate performances of the supercapacitor.

Inserting other conductive materials in MXene interlayer is an effective strategy to avoid the self-agglomeration [9]. It has been demonstrated that the intercalation of graphene sheets in the interlayer of MXene flakes can

Supplementary Information The online version contains supplementary material available at https://doi.org/10.1007/s12598-021-01935-6.

Z. Cai, Y.-F. Ma*, M. Wang*, Z.-M. Tong, L.-T. Xiao, S.-T. Jia, X.-Y. Chen
State Key Laboratory of Quantum Optics and Quantum Optics Devices, Collaborative Innovation Center of Extreme Optics, Institute of Laser Spectroscopy, Shanxi University, Taiyuan 030006, China
e-mail: mayifei@sxu.edu.cn

M. Wang
e-mail: wangmei@sxu.edu.cn

A.-N. Qian
Institute of Resources and Environment Engineering, Shanxi University, Taiyuan 030006, China

X.-Y. Chen
Department of Microsystems, Faculty of Technology, Natural Sciences and Maritime Sciences, University of Southeast Norway, Borre N3184, Norway

effectively inhibit the self-restacking of the MXene [10]. However, the graphene is an impermeable material that cannot allow the electrolyte ions to permeate uprightly, resulting in tortuous ion transport pathways in the MXene/graphene electrode, thereby affecting the rate performance and capacitive properties of the MXene/graphene electrodes. In this circumstance, Liu et al. used holey graphene (HG) as a spacer to expand the interlayer of the MXene and accelerate the diffusion of electrolyte ions, improving the capacitance and rate performances of the MXene electrodes [11]. However, the ion transmission channels in the electrodes have not been scrupulously steered.

In the MXene/graphene-based film electrode, desirable electrochemical performances depend on fast access of the electrolyte ions to the surface of the active materials. The ion diffusion in the layer-by-layer MXene-based electrode is contingent on the interlayer distance and intralayer distance of the MXene nanosheets, which can be engineered by the amount of the holey graphene spacer and size of the MXene nanosheets. Hence, the capacitive properties and rate performances of the MXene/HG could be further improved by gaining insight into the engineering of the electrolyte ion transportation channels.

In this work, we precisely designed the ion channels by engineering the size of monolayer MXene sheets and the amount of HG nanosheets. The monolayer MXene sheets with different sizes were achieved by different ultrasonic methods, by which different sonication powers were applied. Flexible and freestanding MXene/HG supercapacitor electrodes with different MXene sizes and HG contents were obtained by a vacuum-assisted filtration process. Tested as supercapacitor electrodes, the MXene/HG with small size MXene sheets delivers the highest gravimetric capacitance of 446 $F{\cdot}g^{-1}$ at 2 $mV{\cdot}s^{-1}$ and an impressive rate capability with rate retention of 78%. In addition, the symmetric MXene/HG supercapacitors demonstrate desirable gravimetric energy density & power density and remarkable cyclic ability, indicating its great potential for superior capacitive energy storage devices.

2 Experimental

2.1 Synthesis of MXene

$Ti_3C_2T_x$ MXene was synthesized following the previously reported process with some modification [12]. Briefly, 1 g LiF powder (Macklin, 99.99%) and 1 g Ti_3AlC_2 powder (Forsman Scientific, 98%, < 38 μm) were successively added to 20 ml 9 $mol{\cdot}L^{-1}$ HCl solution (Sinopharm Chemical Reagent, 36 wt%–38 wt%) with an interval of 5 min, followed by stirring at 1000 $r{\cdot}min^{-1}$ for 24 h at 35 °C. Then, the mixture was centrifuged at 3500 $r{\cdot}min^{-1}$ for 5 min and rinsed with deionized (DI) water several times until the pH reaches neutral. The mixture was filtrated to obtain the multilayer MXene powder and then dried in air for 24 h. The yield of ~ 92% was obtained. Afterward, an ultrasonic process was applied to form a MXene dispersion with a concentration of 0.5 $mg{\cdot}ml^{-1}$ (25 mg multilayer MXene powder in 50 ml DI water) [13]. Monolayer MXene with an average flake size about 1.7 μm was obtained from under bath sonication system (Scientz, IID) at 35 kHz for 30 min, which is named as large MXene (L-MXene). The monolayer MXene with small flakes of about 0.4 μm was obtained with a probe sonication system (Scientz, SB-4200 DTD) at 400 W for 30 min, which is named as small MXene (S-MXene).

2.2 Synthesis of HG

The HG was synthesized according to our previous report [14]. In brief, the GO aqueous dispersion, purchased from Global Graphene Group (10 $mg{\cdot}ml^{-1}$), was diluted to 2 $mg{\cdot}ml^{-1}$. 0.1 ml H_2O_2 aqueous solution (Aladdin, 30%) was added into 20 ml GO dispersion (2 $mg{\cdot}ml^{-1}$). Afterward, the mixture was transferred to a 50 ml Teflon-lined steel autoclave and reacted at 180 °C for 6 h. The above mixture was filtrated and washed with DI-water several times to remove the residual H_2O_2 and freeze-dried to obtain the HG powder. The HG solution (1 $mg{\cdot}ml^{-1}$) was obtained by dispersing 10 mg HG powder in 10 ml DI water.

2.3 Fabrication of MXene/HG films

Firstly, 12.5 μl HG aqueous dispersion (1 $mg{\cdot}ml^{-1}$) was added into a 50 ml MXene dispersion (0.5 $mg{\cdot}ml^{-1}$). The volumes of the HG and MXene suspensions used for preparing MXene/HG films with different mass ratios are listed in Table S1. Then, the above mixtures were further dispersed and mixed by a bath sonication system at 20 kHz for 30 min. The MXene/HG solution was then vacuum-filtered using a Nylon membrane filter (Whatman Germany, 47 mm in diameter, 0.2 μm in pore size), followed by a vacuum-drying treatment at 25 °C for 12 h. After peeling from the Nylon membrane filter, a freestanding MXene/HG film was obtained. The MXene/HG films are denoted as L-MXene/HG and S-MXene/HG depending on the flake size of the MXene. The MXene/HG films are named as $MXene/HG_{0.05}$ and $MXene/HG_{0.10}$, respectively, representing the HG mass ratio of 0.05 and 0.10 in the MXene/HG film.

2.4 Materials characterizations

Morphology of the films was observed by a scanning electron microscope (SEM, HITACHI SU-8010). The interlayer spacing was detected by X-ray diffraction (XRD, X'Pert PRO MPD) with a 2θ ranging from 5° to 90° and a scanning speed of 5 (°)·min^{-1}. Raman spectra were recorded on a Horiba Scientific LabRAM HR Evolution with a laser operating at 523 nm. The electrochemical properties of the electrodes were characterized by an electrochemical workstation (Biologic, VSP-300). The surface area was measured by the Brunauer–Emmett–Teller (BET) method, using nitrogen gas adsorption–desorption isotherms at 77 K.

2.5 Electrochemical measurements

A three-electrode system was equipped with 1 mol·L^{-1} H_2SO_4 aqueous electrolyte. The MXene-based films, an Ag/AgCl (3 mol·L^{-1} KCl) electrode and a Pt plate were used as working, reference and counter electrodes, respectively. The operation potential was carried out from −0.2 to 0.6 V. The symmetric supercapacitors were assembled using two MXene/HG films with equal mass loading and glass fiber as a separator, in which the operation potential window is applied at −0.5 to 0.5 V. The electrochemical impedance spectroscopy (EIS) measurements with a frequency range from 0.01 Hz to 100 kHz were performed. The gravimetric specific capacitances (C_m, F·g^{-1}) from the galvanostatic charge/discharge (GCD) curves were calculated by Eq. (1):

$$C_m = It/\Delta Vm \quad (1)$$

where I is discharge current (A), t is discharge time (s), ΔV is the potential change in discharge process (V), and m is the mass of the working electrode (g) [15]. The gravimetric capacitances (C_m, F·g^{-1}) were calculated by Eq. (2):

$$C_m = 1/2m\Delta Vv \int i dV \quad (2)$$

where v represents the potential scan rate (mV·s^{-1}), i is the current (A), and $\int i dV$ is the integrated area of the enclosed CV curves. The gravimetric energy density (E_m, Wh·kg^{-1}) and power density (P_m, W·kg^{-1}) of symmetric supercapacitor were calculated based on Eqs. (3, 4):

$$E_m = C_m\Delta V^2/2 \times 3.6 \quad (3)$$

$$P_m = E_m \times 3600/\Delta t \quad (4)$$

3 Results and discussion

The MXene was synthesized from Ti_3AlC_2 by selectively etching the Al atoms by the LiF/HCl solution. After the etching process, an obvious structure change from Ti_3AlC_2 to MXene can be observed in Fig. S1, in which the MXene shows a delaminated structure. The delamination is caused by the Al removal and the intercalation of Li^+ in the interspacing. Then, the further exfoliation was realized by sonication processes to fabricate MXene monolayers. Two kinds of sonication systems, a probe sonication system and a bath sonication system, were utilized to exfoliate the MXene, in which the probe sonication system has a higher energy output than the bath sonication system. As a result, the monolayer MXene are obtained with small flake size (∼ 0.4 μm) which is shattered by strong vibration of the probe sonication system (Figs. 1a and S1). While large flake size of 1.7 μm is obtained with a bath sonication system (Figs. 1b and S1). Holes in the HG flakes are formed by a hydrothermal treatment with H_2O_2 (Fig. 1c, d). In addition, atomic force microscopy (AFM) images of the MXene flakes in Fig. S2 exhibit a flat sheet morphology, and the thicknesses are obtained as 1.7 nm (S-MXene) and 1.9 nm (L-MXene), accordant with the thickness of the monolayer MXene flakes. AFM analysis confirms the successful synthesis of monolayer MXene with our process.

The cross-sectional images of the MXene and MXene/HG composite films are illustrated in Fig. 2a, b. All the films exhibit similar layered structures with the thickness of ∼ 5 μm. The HG nanosheets are too small to be observed and the addition of different ratios of HG does not influence the stacked structure. In addition, the surfaces of the MXene and MXene/HG films exhibit abundant wrinkles with no morphology change after inserting HG nanosheets, as shown in Fig. S3. The bonding states and crystalline structure of the MXene and MXene/HG films were analyzed by Raman spectra and XRD patterns. As shown in Fig. 2c, the A_{1g} symmetry out-of-plane vibrations of Ti and C atoms are represented by the modes at 199 and 720 cm^{-1}, respectively. Meanwhile, the peaks at 281, 390 and 618 cm^{-1} represent the E_g group vibrations of Ti atoms, C atoms and terminal group atoms, respectively. After incorporating HG nanosheets, the two obvious broad peaks at 1350 and 1582 cm^{-1} can be assigned to D and G bands of graphitic carbon [16] indicating the existence of holey graphene in the MXene/HG films.

Figure 2d shows XRD patterns of the MXene and the MXene/HG films. XRD was carried out to characterize the interlayer distance of the MXene and MXene/HG films, as shown in Fig. 2d. The (002) diffraction peak of the pure MXene film (L-MXene) appears at around 7.11°, indicating the interlayer spacing of about 1.38 nm. After HG is incorporated into the L-MXene interlayer, it is obvious that XRD pattern of the L-MXene/HG films shows a left shift, which proves that the interlayer spacing of the L-MXene/HG film is expanded [17]. Meanwhile, the (002) diffraction

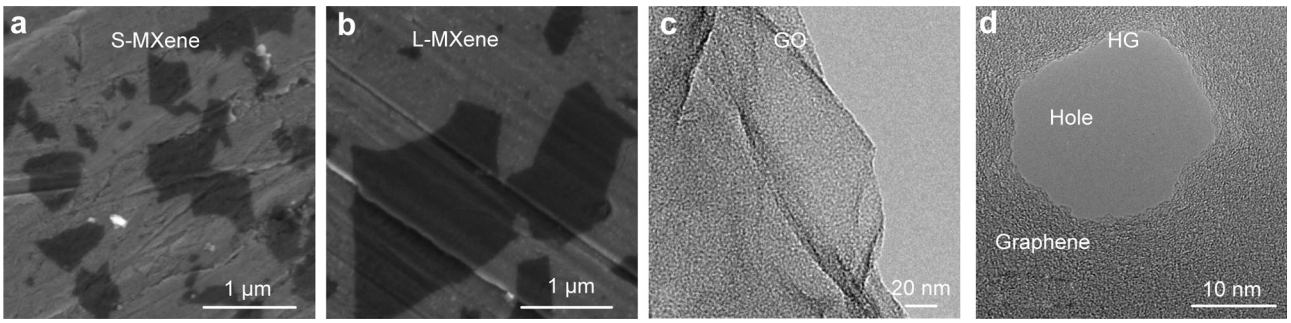

Fig.1 SEM images of monolayer MXene nanoflakes with **a** small flake sizes and **b** large flake sizes; TEM images of **c** GO and **d** HG

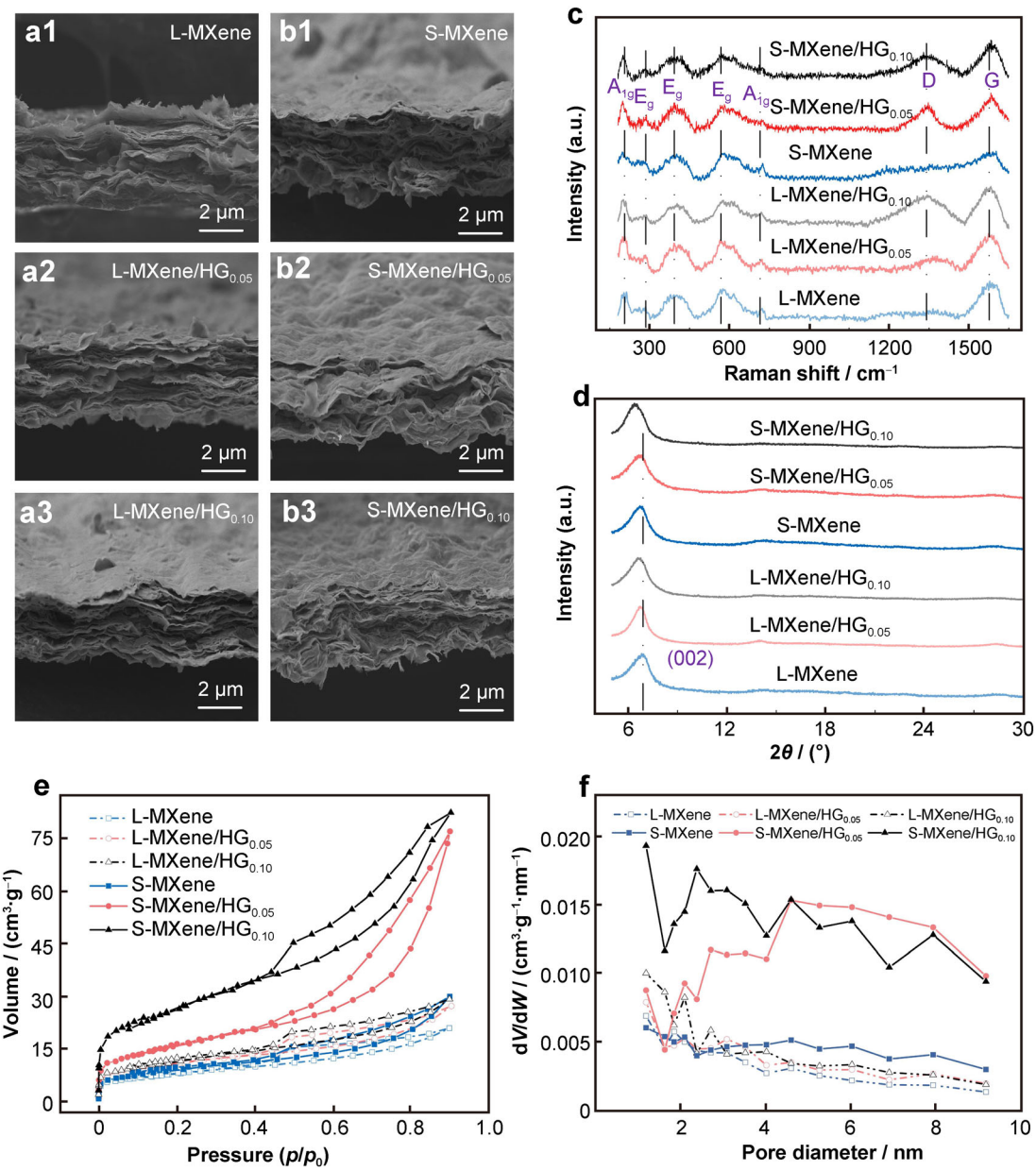

Fig. 2 Cross-sectional SEM images of **a1**–**a3** L-MXene and L-MXene/HG films and **b1**–**b3** S-MXene and S-MXene/HG films; **c** Raman spectra and **d** XRD patterns of MXene and MXene/HG films; **e** nitrogen adsorption and desorption isotherms of MXene and MXene/HG; **f** BJH pore size distribution of MXene and MXene/HG

peak of the pure MXene film (S-MXene) appears at around 6.76°, which refers to the interlayer spacing of 1.58 nm, indicating a larger interlayer distance than that of L-MXene. With the increase in the HG content, the (002) diffraction peak also shows a left shift, referring to an enlarged interlayer spacing and demonstrating the successful intercalation of the HG in the MXene interlayers.

Figure S4a illustrates the densities of the pure MXene and MXene/HG films. The density of the L-MXene is similar to that of S-MXene, while the density of MXene/HG films was decreased due to the involvement of the low-density HG. However, the square electrical resistance of the S-MXene film is higher than that of L-MXene due to the pronounced contact resistance between the small flakes, as shown in Fig. S4b. Moreover, the electrical resistance of the MXene/HG films increases with the addition of HG content derived from the high resistance of the HG [18].

Figure 2e characterizes the nitrogen adsorption and desorption isotherms of the MXene and MXene/HG, confirming that S-MXene-based films provide higher specific surface area than L-MXene-based films. Impressively, S-MXene/$HG_{0.05}$- and S-MXene/$HG_{0.10}$-based films exhibit representative "Type IV" hysteresis in the mesopore region, indicating the existence of mesopores with a minor fraction of micropores. This conclusion can also be demonstrated by the pore size distribution obtained by the Barrett-Joyner-Halenda (BJH) method in Fig. 2f. The L-MXene-based films and S-MXene film have the similar pore distribution, while the amount of the mesopores increases sharply in S-MXene/$HG_{0.05}$ and S-MXene/$HG_{0.10}$ after the introduction of the HG in S-MXene. Therefore, the S-MXene/$HG_{0.05}$ and S-MXene/$HG_{0.10}$ obtain high BET surface area of 57.27 and 62.39 $m^2 \cdot g^{-1}$, respectively (Fig. S5). BET result is consistent with XRD measurement that the insertion of the HG flakes can avoid the lamellar accumulation of MXene flakes and increase the interlayer spacing so as to improve the specific surface area.

The electrochemical properties of the MXene and MXene/HG films were tested in a three-electrode system in a 1 $mol \cdot L^{-1}$ H_2SO_4 electrolyte. Firstly, the cyclic voltammetry (CV) profiles are depicted in Fig. 3a at a scan rate of 200 $mV \cdot s^{-1}$, where the redox peaks indicate the pseudo-capacitive behavior of MXene in the MXene and MXene/HG electrodes [19]. Obviously, the S-MXene/$HG_{0.05}$ exhibits the largest integration area, corresponding to the highest gravimetric capacitance. The CV curves of the MXene and MXene/HG films at scan rates from 2 to 500 $mV \cdot s^{-1}$ were tested to investigate their electrochemical properties (Fig. S6), and the specific capacitances are plotted in Fig. 3b. Despite the capacitance, the S-MXene also possesses better rate performance than the L-MXene. The S-MXene shows high gravimetric capacitance of 357 $F \cdot g^{-1}$ at 2 $mV \cdot s^{-1}$ and 214 $F \cdot g^{-1}$ at 500 $mV \cdot s^{-1}$, with a capacitance retention of 60%. However, the L-MXene shows gravimetric capacitance of 228 $F \cdot g^{-1}$ at 2 $mV \cdot s^{-1}$ and 86 $F \cdot g^{-1}$ at 500 $mV \cdot s^{-1}$ with a capacitance retention of only 38%. The small lamella has more defects, higher specific surface area, and larger spacing between the interlayers, thereby resulting in a higher capacitance and a better capacitance retention. The addition of moderate HG further enhances the gravimetric capacitance and rate capabilities so that the L-MXene/$HG_{0.05}$ demonstrates a capacitance of 356 $F \cdot g^{-1}$ at 2 $mV \cdot s^{-1}$ with a retention of 65% at 500 $mV \cdot s^{-1}$, while the S-MXene/$HG_{0.05}$ exhibits the highest capacitance of 446 $F \cdot g^{-1}$ at the scan rate of 2 $mV \cdot s^{-1}$ as well as the highest capacitance retention of 77.5%. In addition, as shown in Table S2, the volumetric capacitances of the electrodes are also significantly enhanced after HG intercalation, and the S-MXene/$HG_{0.05}$ electrode provides an impressive volumetric capacitance of 1274.16 $F \cdot cm^{-3}$.

In addition, the dynamic sweep voltammetry was employed to analyze the surface control dynamics, and the results are shown in Fig. 3c, d. The capacitive- and diffusion-controlled capacitance contributions were determined as follows:

$$i(V) = k_1 v + k_2 v^{1/2} \tag{5}$$

where the i (V) represents the current at a specific potential, v is the voltage scan rate, $k_1 v$ and $k_2 v^{1/2}$ are the capacitive and diffusion-controlled current contributions, respectively [20].

By calculating i (V)/$v^{1/2}$ and $v^{1/2}$ at different scanning rates, the k_1 values can be identified to determine the fraction of the current originating from the capacitive-controlled process. As shown in Fig. 3c, the capacitive control capacitance (the shaded portion) at the scan rate of 200 $mV \cdot s^{-1}$ of the S-MXene/$HG_{0.05}$ is determined by synthetically calculating k_1. Table S3 shows the capacitive-controlled capacitances of the electrodes at the scan rate of 200 $mV \cdot s^{-1}$. It can be concluded that the capacitive-controlled capacitance of the S-MXene/$HG_{0.05}$ is the highest (92.9%) and the capacitance of the MXene can be almost fully utilized with the aid of HG by enlarging the interspacing. Figure 3d illustrates the capacitive-controlled capacitance components of the S-MXene/$HG_{0.05}$ electrode at different scan rates. The high capacitive contribution reveals that the primary capacitance is contributed by the capacitive control process.

To further study the electrochemical performances of the MXene/HG-based electrodes, the symmetric supercapacitors were assembled based on MXene and MXene/HG electrodes with glass fiber films as the separator in a 1 $mol \cdot L^{-1}$ H_2SO_4 aqueous electrolyte. The as-fabricated device showcases a highly capacitive behavior, including a rectangular CV shape and rapid current response upon

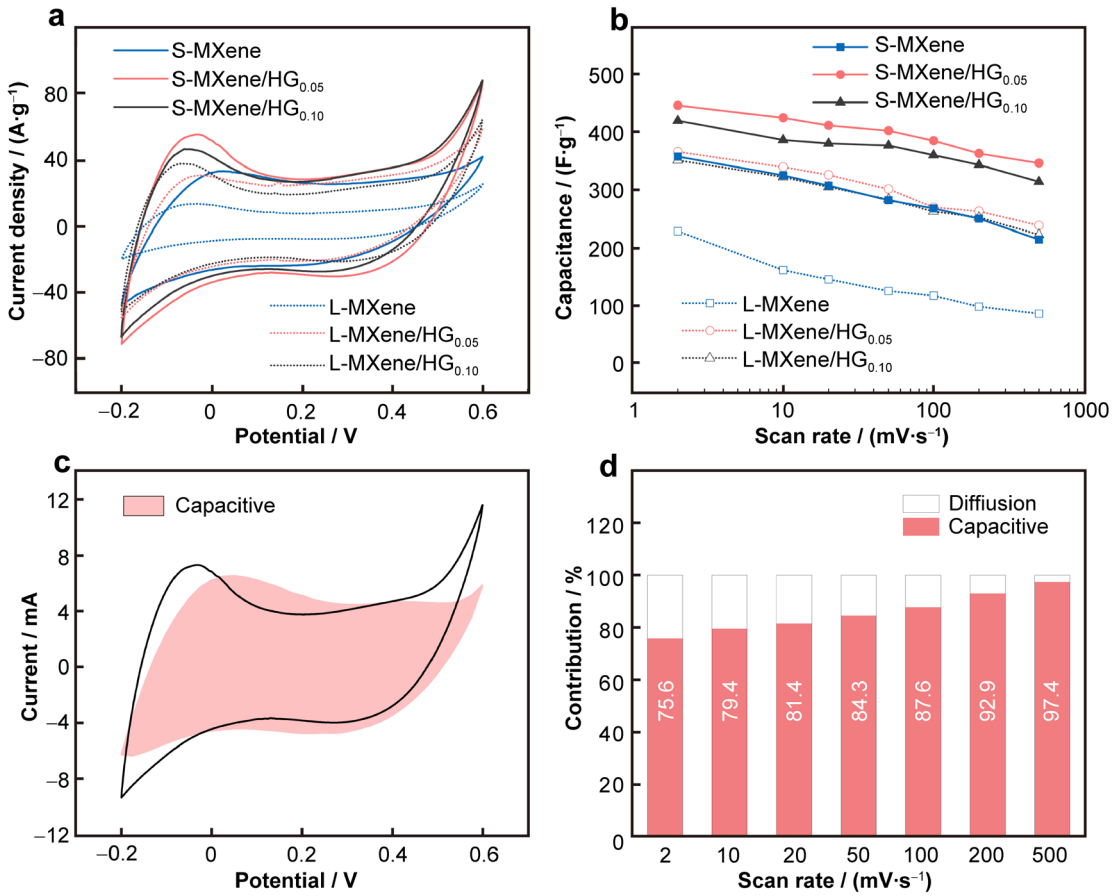

Fig. 3 **a** CV profiles of pure MXene films and MXene/HG films at a scan rate of 200 mV·s^{-1}; **b** gravimetric capacitance of MXene films and MXene/HG films at different scan rates; **c** CV curve of S-MXene/HG$_{0.05}$ at 200 mV·s^{-1}, showing capacitive- (shaded) and diffusion-controlled process; **d** capacitive- and diffusion-controlled capacitance contribution of S-MXene/HG$_{0.05}$ at different scan rates

voltage reversal, as shown in Fig. 4a. The CV curves of all the MXene- and MXene/HG-based supercapacitors can still maintain the shape even at a high scan rate up to 1000 mV·s^{-1} (Fig. S7). The gravimetric capacitance calculated from the CV curves is plotted in Fig. 4b, showing that the S-MXene film presents better capacitance and capacitance retention than the L-MXene, coincident with the result obtained from three-electrode CV analysis (Fig. S8). Specially, the S-MXene/HG$_{0.05}$-based supercapacitor shows the highest capacitance of 159 F·g^{-1} at the scan rate of 20 mV·s^{-1} with a capacitance retention of 70.48% to the scan rate of 1000 mV·s^{-1}.

Figure 4c shows GCD curves of the MXene and MXene/HG films at the current density of 2 A·g^{-1}. The S-MXene/HG$_{0.05}$ film shows the highest capacitance referring from the longest discharge time in the GCD curves, which is consistent with the CV analysis. Figure S9 shows the GCD curves of all the MXene- and MXene/HG-based symmetric supercapacitors at different current densities. The specific gravimetric capacitances of the MXene and MXene/HG films are obtained at different current densities (Fig. 4d), where the rate retention of the supercapacitors are also presented in Fig. S10. The S-MXene/HG$_{0.05}$ shows the highest capacitance of 106.86 F·g^{-1} at 0.5 A·g^{-1} and 86.65 F·g^{-1} when the current density is up to 10 A·g^{-1}. The rate retention of the S-MXene/HG$_{0.05}$ film increases from 62.9% to 81.1% (from 0.5 to 10.0 A·g^{-1}) with the addition of HG, presenting a better rate capability than L-MXene and other MXene-based supercapacitors [21].

The rate performances of the MXene and MXene/HG electrodes can be explained by the schematic diagram of the ion transportation in Fig. 4e. The electrolyte ions in the L-MXene require a longer transportation pathway than in the S-MXene. Inserting the HG between the MXene flakes can effectively increase the choice of ion transport channels, in which the ions can permeate the HG through the holes in HG, thereby enhancing the rate performances of S-MXene/HG.

Figure 5a presents the electrochemical impedance spectroscopy (EIS) with the Nyquist plot and equivalent circuit of the MXene-based electrodes [22], where R_1

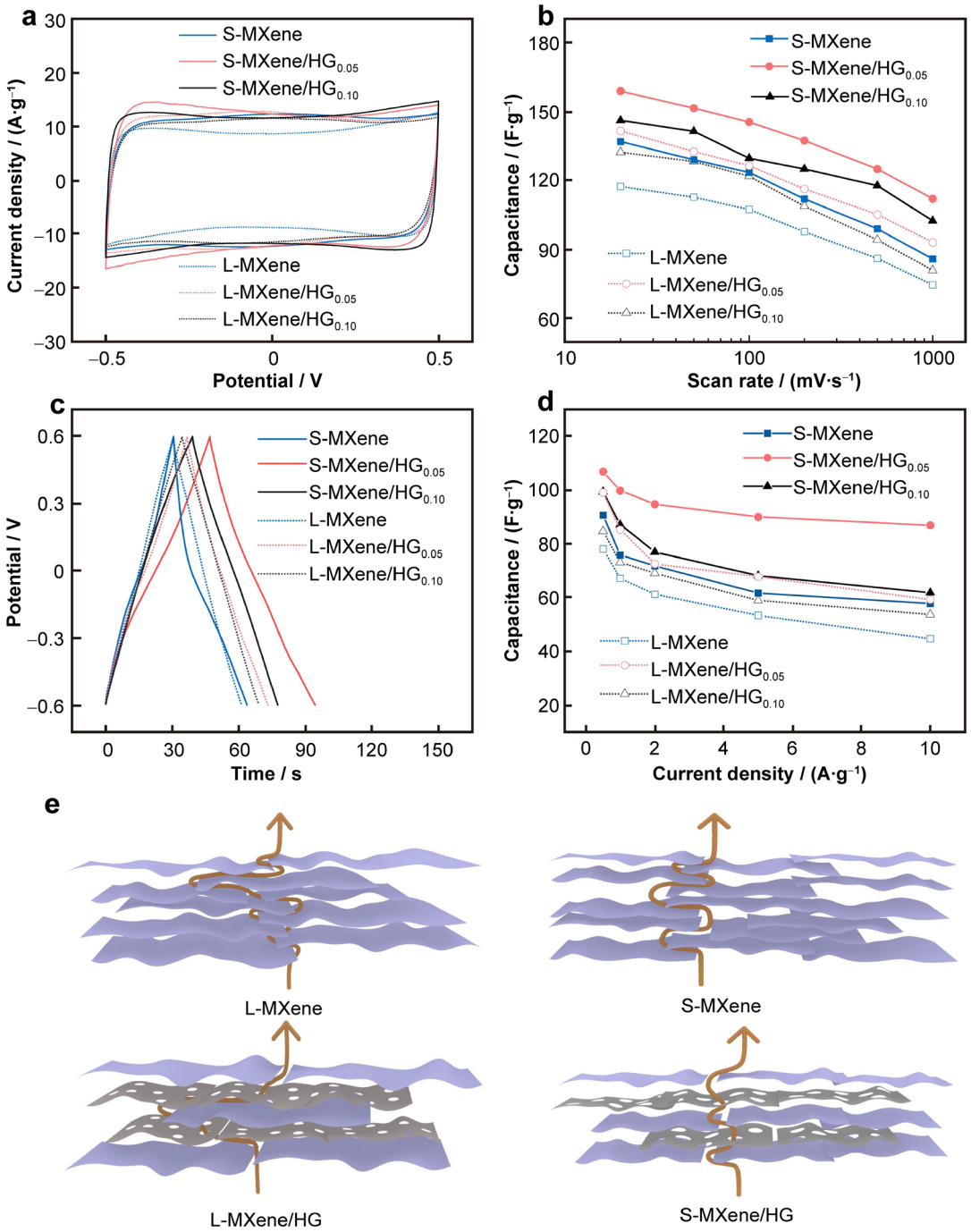

Fig. 4 Electrochemical characterizations of MXene and MXene/HG based symmetric supercapacitors: **a** CV profiles at a scan rate of 200 mV·s^{-1}; **b** gravimetric capacitances at different scan rates; **c** GCD curves at current density of 2 A·g^{-1}; **d** gravimetric capacitances at different current densities; **e** schematic diagram of electrolyte ion transportation pathway in MXene and MXene/HG films

represents the internal impedance (the first X-intercept), R_{ct} is the interfacial charge-transfer resistance (the diameter of the semi-circle arc), W is the Warburg diffusional impedance controlled by mass-transfer. The detailed fitting results are presented in Table S4. The pure MXene film shows a lower internal resistance than the MXene/HG films, which can be attributed to the relatively high resistance of HG derived from a plenty of defects (holes). The addition of HG avoids the self-accumulation of MXene and provides more ion penetration channels. Therefore, the interfacial charge-transfer resistance of the MXene/HG films is evidently lower than that of MXene films,

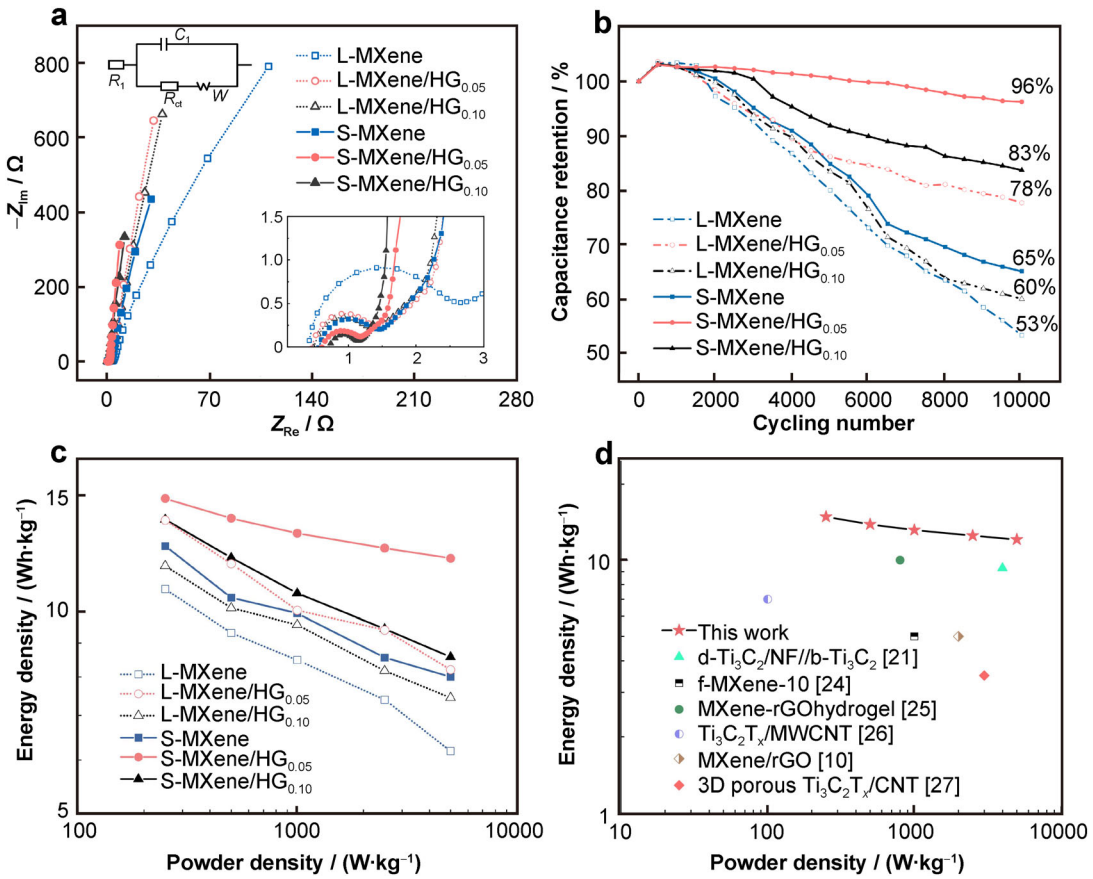

Fig. 5 **a** Nyquist plots of MXene and MXene/HG electrodes and (inset) high-frequency region and equivalent circuit; **b** capacitance retention rate of symmetric supercapacitors based on MXene and MXene/HG electrodes after 10,000 cycles at a current density of 5 A·g^{-1}; **c** gravimetric energy and power densities of assembled symmetric supercapacitors based on MXene and MXene/HG films; **d** gravimetric energy and power densities of S-MXene/HG$_{0.05}$ based symmetric supercapacitor in comparison with reported MXene-based supercapacitors

demonstrating faster ion transportation in the MXene/HG electrodes after embedding the HG. The intersection point of a line with an inclination angle of 45° on the low frequency region in the Nyquist plot with the *X*-axis is defined as the value of the equivalent series resistance (ESR) [23]. The S-MXene/HG$_{0.05}$ electrode exhibits the lowest ESR, which greatly boosts the supercapacitive ability and rate performances. Figure 5b demonstrates an excellent cyclic performance of the S-MXene/HG$_{0.05}$ electrode with 96% retention after 10,000 cycles at a specific current density of 5 A·g^{-1}, whereas the other electrodes exhibit significant capacitance attenuation after 10,000 cycles. SEM images of the electrode materials surface after 10,000 cycles are shown in Fig. S11. The surface of the MXene flakes becomes rough, which has been revealed to be caused by the coarsening of structures [24, 25]. However, the S-MXene/HG$_{0.05}$ electrode is relatively less passivated, further demonstrating its desirable cyclic performances.

Figure 5c shows the gravimetric energy and power densities of the assembled symmetric supercapacitors based on the MXene and MXene/HG electrodes, which can better demonstrate the practical operational potential of the devices. The S-MXene/HG$_{0.05}$-based symmetric supercapacitor obtains a maximum gravimetric energy density of 14.84 Wh·kg^{-1} at a power density of 250 W·kg^{-1}, retaining 12.06 Wh·kg^{-1} at an excellent power density of 5000 W·kg^{-1}. Figure 5d compares the energy density and power density of our S-MXene/HG$_{0.05}$ supercapacitor with other reported MXene-based supercapacitors, including d-Ti$_3$C$_2$/NF//b-Ti$_3$C$_2$ [21], f-MXene-10 [26], MXene-rGO hydrogel [27], Ti$_3$C$_2$T$_x$/MWCNT [28], MXene/rGO [10] and three-dimensional porous Ti$_3$C$_2$T$_x$/carbon nanotubes [29]. Our S-MXene/HG$_{0.05}$-based supercapacitor exhibits superior energy densities than other MXene-based supercapacitors, deriving from the scrupulous design of the ion transmission channels.

4 Conclusion

In summary, the electrolyte ion transmission channels in the MXene/HG electrode were scrupulously designed and engineered by controlling the MXene lamellar size and inserting the HG. The S-MXene/$HG_{0.05}$ electrode exhibits excellent gravimetric capacitance of 446 $F{\cdot}g^{-1}$ at the scan rate of 2 $mV{\cdot}s^{-1}$. Compared with that of pure MXene, the rate capability of the S-MXene/$HG_{0.05}$ electrode increases from 38.0% to 77.5%. The symmetric supercapacitor demonstrates a superior gravimetric energy density of 14.84 $Wh{\cdot}kg^{-1}$ with an excellent cyclic stability with 96% of the capacitance retention after 10,000 cycles. This work provides a concept of two-dimensional material-based electrode design with an easy ion channel engineering method for superior supercapacitive performances.

Acknowledgements This study was financially supported by the National Key R&D Program of China (No. 2017YFA0304203), the National Natural Science Foundation of China (Nos. 21805174 and 51902190), the Key Research and Development Program of Shanxi Province for International Cooperation (No. 201803D421082), the Scientific and Technological Innovation Programs of Higher Education Institutions in Shanxi (Nos. 2019L0013 and 2019L0018), Shanxi Scholarship Council of China (No. 2021-004), the Program of Introducing Talents of Discipline to Universities (No. D18001), the Changjiang Scholars and Innovative Research Team at the University of Ministry of Education of China (No. IRT_17R70) and the Fund for Shanxi "1331 Project."

Declarations

Conflict of interests The authors declare that they have no conflict of interest.

References

[1] Hu M, Li Z, Zhang H, Hu T, Zhang C, Wu Z, Wang X. Self-assembled $Ti_3C_2T_x$ MXene film with high gravimetric capacitance. Chem Commun. 2015;51:13531.
[2] Yang CZ, Huang HJ, He HY, Yang L, Jiang QG, Li WH. Recent advances in MXene-based nanoarchitectures as electrode materials for future energy generation and conversion applications. Coord Chem Rev. 2021;435:213806.
[3] Huang HJ, Wei YJ, Yang Y, Yan MM, He HY, Jiang QG, Yang XF, Zhu JX. Controllable synthesis of grain boundary-enriched Pt nanoworms decorated on graphitic carbon nanosheets for ultrahigh methanol oxidation catalytic activity. J Energ Chem. 2021;57:601.
[4] Yang CZ, Jiang QG, Liu H, Yang L, He HY, Huang HJ, Li WH. Pt-on-Pd bimetallic nanodendrites stereoassembled on MXene nanosheets for use as high-efficiency electrocatalysts toward the methanol oxidation reaction. J Mater Chem A. 2021;9:15432.
[5] Li H, Hou Y, Wang F, Lohe MR, Zhuang XD, Niu L, Feng XL. Flexible all-solid-state supercapacitors with high volumetric capacitances boosted by solution processable mxene and electrochemically exfoliated graphene. Adv Energy Mater. 2017;7(4):1601847.
[6] Alhabeb M, Maleski K, Anasori B, Lelyukh P, Clark L, Sin S, Gogotsi Y. Guidelines for synthesis and processing of two-dimensional titanium carbide ($Ti_3C_2T_x$ MXene). Chem Mater. 2017;29(18):7633.
[7] Yang L, Zheng W, Zhang P, Chen J, Tian WB, Zhang YM, Sun ZM. MXene/CNTs films prepared by electrophoretic deposition for supercapacitor electrodes. J Electroanal Chem. 2018;830–831:1.
[8] Salles P, Quain E, Kurra N, Sarycheva A, Gogotsi Y. Automated scalpel patterning of solution processed thin films for fabrication of transparent MXene microsupercapacitors. Small. 2018;14(44):1802864.
[9] Zhao MQ, Ren CE, Ling Z, Lukatskaya MR, Zhang C, Van Aken KL, Barsoum MW, Gogotsi Y. Flexible MXene/carbon nanotube composite paper with high volumetric capacitance. Adv Mater. 2015;27(2):339.
[10] Yan J, Ren CE, Maleski K, Hatter CB, Anasori B, Urbankowski P, Sarycheva A, Gogotsi Y. Flexible MXene/graphene films for ultrafast supercapacitors with outstanding volumetric capacitance. Adv Funct Mater. 2017;27(30):1701264.
[11] Fan ZM, Wang YS, Xie ZM, Wang DL, Yuan Y, Kang HJ, Su BL, Cheng ZJ, Liu YY. Modified MXene/holey graphene films for advanced supercapacitor electrodes with superior energy storage. Adv Sci. 2018;5(10):1800750.
[12] Qian AN, Seo JY, Shi H, Lee JY, Chung CH. Surface functional groups and electrochemical behavior in dimethyl sulfoxide-delaminated $Ti_3C_2T_x$ MXene. Chemsuschem. 2018;11(21):3719.
[13] Malaki M, Maleki A, Varma RS. MXenes and ultrasonication. J Mater Chem A. 2019;7(18):10843.
[14] Yun MC, Ma YF, Cai Z, Ji HM, Han JM, Wang M, Tong ZM, Xiao LT, Jia ST, Chen XY. Holey graphene interpenetrating networks for boosting high-capacitive Co_3O_4 electrodes via an electrophoretic deposition process. Ceram Int. 2021;47(19):27210.
[15] Wang M, Oh J, Ghosh T, Hong S, Nam G, Hwang T, Nam JD. An interleaved porous laminate composed of reduced graphene oxide sheets and carbon black spacers by in situ electrophoretic deposition. RSC Adv. 2014;4(7):3284.
[16] Wang M, le Duong D, Mai NT, Kim S, Kim Y, Seo H, Kim YC, Jang W, Lee Y, Suhr J, Nam JD. All-solid-state reduced graphene oxide supercapacitor with large volumetric capacitance and ultralong stability prepared by electrophoretic deposition method. ACS Appl Mater Interf. 2015;7(2):1348.
[17] Mashtalir O, Naguib M, Mochalin VN, Dall'Agnese Y, Heon M, Barsoum MW, Gogotsi Y. Intercalation and delamination of layered carbides and carbonitrides. Nat Commun. 2013;4:1716.
[18] Jiang Q, Kurra N, Maleski K, Lei Y, Liang H, Zhang Y, Gogotsi Y, Alshareef HN. On-chip MXene microsupercapacitors for AC-line filtering applications. Adv Energy Mater 2019;9(26):1901061.
[19] Shao H, Lin Z, Xu K, Taberna PL, Simon P. Electrochemical study of pseudocapacitive behavior of $Ti_3C_2T_x$ MXene material in aqueous electrolytes. Energy Stor. 2019;18:456.
[20] Chen XF, Zhu YZ, Zhang M, Sui JY, Peng WC, Li Y, Zhang GL, Zhang FB, Fan XB. N-Butyllithium-treated $Ti_3C_2T_x$ MXene with excellent pseudocapacitor performance. ACS Nano. 2019;13(8):9449.
[21] Guo J, Zhao YY, Liu AM, Ma TL. Electrostatic self-assembly of 2D delaminated MXene (Ti_3C_2) onto Ni foam with superior electrochemical performance for supercapacitor. Electrochim Acta. 2019;305:164.
[22] Ma J, Cheng YJ, Wang L, Dai XH, Yu F. Free-standing $Ti_3C_2T_x$ MXene film as binder-free electrode in capacitive deionization with an ultrahigh desalination capacity. Chem Eng J. 2020;384:123329.
[23] Zhang JZ, Seyedin SY, Gu ZJ, Yang WR, Wang XG, Razal JM. MXene: a potential candidate for yarn supercapacitors. Nanoscale. 2017;9(47):18604.

[24] Qian AN, Hyeon SE, Seo JY, Chung CH. Capacitance changes associated with cation-transport in free-standing flexible $Ti_3C_2T_x$ (T=O, F, OH) MXene film electrodes. Electrochim Acta. 2018;266:86.
[25] Cherevko S, Kulyk N, Chung CH. Nanoporous Pt@Au_xCu_{100-x} by hydrogen evolution assisted electrodeposition of Au_xCu_{100-x} and galvanic replacement of Cu with Pt: electrocatalytic properties. Langmuir. 2012;28(6):3306.
[26] Ran FT, Wang TL, Chen SY, Liu YY, Shao L. Constructing expanded ion transport channels in flexible MXene film for pseudocapacitive energy storage. Appl Surf Sci. 2020;511:145627.
[27] Dutta P, Sikdar A, Majumdar A, Borah M, Padma N, Ghosh S, Maiti UN. Graphene aided gelation of MXene with oxidation protected surface for supercapacitor electrodes with excellent gravimetric performance. Carbon. 2020;169:225.
[28] Navarro-Suárez AM, Van Aken KL, Mathis T, Makaryan T, Yan J, Carretero-González J, Rojo T, Gogotsi Y. Development of asymmetric supercapacitors with titanium carbide-reduced graphene oxide couples as electrodes. Electrochim Acta. 2018;259:752.
[29] Zhang P, Zhu QZ, Soomro RA, He S, Sun N, Qiao N, Xu B. In situ ice template approach to fabricate 3D flexible MXene Film-based electrode for high performance supercapacitors. Adv Funct Mater. 2020;30(47):2000922.